RSC Advances

RSC Publishing

PAPER

View Article Online
View Journal | View Issue

Cite this: *RSC Advances*, 2013, **3**, 9453

Iron-core carbon-shell nanoparticles reinforced electrically conductive magnetic epoxy resin nanocomposites with reduced flammability†

Xi Zhang,[ab] Ouassima Alloul,[a] Jiahua Zhu,[a] Qingliang He,[a] Zhiping Luo,[c] Henry A. Colorado,[d] Neel Haldolaarachchige,[e] David P. Young,[e] T. D. Shen,[f] Suying Wei*[b] and Zhanhu Guo*[a]

Carbon coated iron (Fe@C) nanoparticles successfully served as nanofillers for obtaining magnetic epoxy resin polymer nanocomposites (PNCs). The effects of nanofiller loading level on the rheological behaviors, thermal stability, flammability, dynamic mechanical, mechanical properties, electrical conductivity and magnetic properties were systematically studied. And the curing process of the PNCs was also studied by Fourier transform infrared spectroscopy test. A reduced viscosity was observed in the 1.0 wt% Fe@C/epoxy resin liquid suspension samples and the viscosity was increased with further increasing the Fe@C nanoparticle loading. In the TGA test, the introduction of the Fe@C nanofillers gave a lower onset decomposition temperature of the PNCs. However, a reduced flammability was observed in the PNCs due to the easier char formation from epoxy matrix induced by the Fe@C nanoparticles. The dynamic storage and loss modulii were studied together with the glass transition temperature (T_g) being obtained from the peak of tanδ. Enhanced storage modulus was observed in the PNCs with 20.0 wt% Fe@C nanoparticles. The percolation thresholds of the Fe@C nanoparticles were identified with the study of tensile strength and electrical conductivity. Due to the cavities initiated by the nanoparticles, the PNCs with 5.0 wt% Fe@C nanoparticles showed an increased tensile strength up to 60% compared with pure epoxy. The Fe@C nanofillers could efficiently increase the electrical conductivity of the epoxy matrix, and the particle chain observed in the SEM image of fracture surface indicated the formation of percolated Fe@C nanoparticles in the epoxy matrix. Finally, the Fe@C nanoparticles become magnetically harder after dispersing in epoxy due to the decreased interparticle dipolar interaction, which arises from the enlarged nanoparticle spacer distance for the single domain nanoparticles.

Received 14th March 2013,
Accepted 22nd March 2013

DOI: 10.1039/c3ra41233d

www.rsc.org/advances

1. Introduction

Polymer nanocomposites (PNCs) are attracting ever increasing interests owing to their flexible structural design and impressive electrical,[1] mechanical[2] and magnetic properties with significantly reduced weight.[1] Recently, magnetic PNCs gained more attention due to their unique applications including microwave absorption,[3] electromagnetic interference (EMI) shielding[4] and biochemical separation fields.[5] Epoxy as one of the most important engineered polymers is popular due to its wide applications including structural materials, tissue substitutes,[6] anti-corrosion coatings[7] and flame retardant additives.[8] However, the industrial deployments of epoxy demand special functions suitable for applications in specific fields. For instance, electrically conductive epoxy with metal fillers can be used as electronic packaging materials[9] and a significantly enhanced tensile strength is observed in epoxy resin reinforced with polyaniline stabilized multi-wall carbon nanotubes.[10]

Magnetic particles, consisting of magnetic elements such as iron, cobalt, nickel and their corresponding oxides, have been the focus of research due to their attractive physicochemical properties, which can offer a great potential either in their bare form or through coating.[11–13] And due to their small dimensions (usually in the range of 1–10 nanometers),[14]

[a]*Integrated Composites Laboratory (ICL), Dan F. Smith Department of Chemical Engineering, Lamar University, Beaumont, TX, 77710, USA. E-mail: zhanhu.guo@lamar.edu; Tel: +1-409-880-7654 (Z.G.)*
[b]*Department of Chemistry and Biochemistry, Lamar University, Beaumont, TX, 77710, USA. E-mail: suying.wei@lamar.edu; Tel: +1-409-880-7976 (S.W.)*
[c]*Department of Chemistry and Physics and Southeastern North Carolina Regional, Microanalytical and Imaging Consortium, Fayetteville State University, Fayetteville, NC, 28301, USA*
[d]*Department of Mechanical and Aerospace Engineering, University of California Los Angeles, Los Angeles, CA, 90095, USA*
[e]*Department of Physics and Astronomy, Louisiana State University, Baton Rouge, LA, 70803, USA*
[f]*Nanostructured & Amorphous Materials Inc., Houston, TX, 77084, USA*
† Electronic supplementary information (ESI) available. See DOI: 10.1039/c3ra41233d

magnetic nanoparticles have demonstrated more efficient interactions with polymers and hence influence the surface energy at the interface.[15] Meanwhile, to overcome easy oxidation and flammability of metallic nanoparticles in air,[1] silica,[16–18] polymer,[19] carbon[20–22] and noble metals[23–25] have been explored to serve as protecting shells. And compared to others, carbon exhibits much higher stability in harsh environments[26] and better biocompatibility.[20]

Generally, magnetic materials are classified into two types, magnetically soft and magnetically hard materials, based on the criterion of remanence and coercivity. Soft magnetic material can be applied in magnetic recording heads and integrated inductor fields[27] and hard magnetic materials become more and more important due to their unique properties allowing to tailor the characteristic properties of the hysteresis loop.[28] Though epoxy resin based magnetic PNCs with iron particles have been fabricated and the PNCs show good microwave absorption in the radar band,[29] epoxy nanocomposites reinforced with iron coated carbon nanoparticles have been rarely reported and are demanding for academic interests and engineering applications.

In this paper, the Fe@C nanoparticles were applied as nanofillers to obtain conductive magnetic epoxy resin nanocomposites. The PNCs with different loading levels were prepared. The curing process of the PNCs was also studied by Fourier transform infrared spectroscopy tests. The rheological behaviors of the uncured samples (liquid phase), including viscosity at steady state, complex viscosity and viscosity storage and loss modulii in oscillation process were studied. And for all the cured samples (solid phase), the thermal stability was studied by thermogravimetric analysis (TGA), flammability and differential scanning calorimeter (DSC) tests. The thermomechanical properties including storage and loss modulii, glass transition temperature were evaluated together with the tensile mechanical properties. The effects of Fe@C nanoparticle loading on the electrical conductivity and magnetic property were systematically assessed as well.

2. Experimental

2.1 Materials

The epoxy resin Epon 862 (bisphenol F epoxy) and EpiCure curing agent W were purchased from Miller-Stephenson Chemical Company, Inc. Core–shell structured Fe@C nanoparticles (carbon shell thickness: 0.5–1 nm), with an average particle size of 25 nm were provided by Nano-structured and Amorphous Materials, Inc. All the materials were used as received without any further treatment.

2.2 Preparation of Fe@C/epoxy resin nanocomposites

Epoxy resin nanosuspensions with 1.0, 5.0, 10.0 and 20.0 wt% Fe@C nanoparticles were prepared. Firstly the specific amount of Fe@C nanoparticles were immersed in epoxy resin (the total weight of epoxy resin and curing agent was fixed to 40.0 g and the loading of Fe@C nanoparticles in epoxy resin was controlled by varying the weight of the Fe@C nanoparticles) without any disturbance overnight so that the resin could wet the nanostructures completely. The mixture was then mechanically stirred (Heidolph, RZR 2041) at a speed of 600 rpm for one hour at room temperature. Curing agent W was added into the above suspension with a weight ratio of monomer/curing agent: 100/26.5 as recommended by the company and the solution was stirred at high-speed (600 rpm) for another one hour at room temperature. In order to remove bubbles in the solution and to prevent the sedimentation of the Fe@C nanoparticles during the curing process, low-speed (200 rpm) mechanical stirring was conducted at 70 °C for 3–4 h in a water bath. Finally, the solution was poured into silicone rubber molds and cured at 120 °C for 5 h and then cooled down naturally to room temperature. The curing cycle of pristine epoxy was the same as used in curing the Fe@C/epoxy nanocomposites.

2.3 Characterization

Rheological behaviors of liquid epoxy resin nanosuspensions. The rheological behaviors of the epoxy resin nanocomposite suspensions were investigated with a rheometer (AR 2000ex, TA Instruments) at shear rates ranging from 0.1 to 500 s^{-1} at 25 °C (the samples were a mixture of only epoxy monomers and nanofillers). A series of measurements were performed in a cone-and-plate geometry with a diameter of 40 mm and a truncation of 64 μm. Dynamic rheological measurements were also performed with a sweeping frequency range between 0.1 and 100 Hz at a low strain (1%), which was justified to be within the linear viscoelastic (LVE) range for these materials. The LVE range was determined by the strain-storage modulus (G') curve within the strain range from 0.01 to 100 at a frequency of 1 rad s^{-1}. Specimens placed between the cone and plate were allowed to equilibrate for approximately two minutes prior to each frequency sweeping.

Thermal characterization of Fe@C/epoxy nanocomposites. The thermal stability of the cured Fe@C/epoxy PNCs was studied by a thermogravimetric analysis (TGA, Q-500, TA instruments). All the samples were heated from 30 to 700 °C with an air flow rate of 60 mL min^{-1} and a heating rate of 10 °C min^{-1}. Differential scanning calorimeter (DSC, Q2000, TA Instruments) measurements were implemented under a nitrogen flow rate of approximately 20 mL min^{-1} at a heating rate of 10 °C min^{-1} from 0 to 300 °C.

Flammability of cured epoxy nanocomposites. The flammability performance was evaluated by using a micro-scale combustion calorimeter (MCC, model ''MCC-2'', Govmark, Farmingdale, New York) according to American Society for Testing and Materials (ASTM D7309 - Method A). The sample ($\sim$3 mg) was heated to a specified temperature using a linear heating rate (1 °C s^{-1}) in a stream of nitrogen flow rate of 80 mL min^{-1}. The thermal degradation products of the sample in nitrogen were mixed with a 20 mL min^{-1} stream of oxygen prior to entering the 900 °C combustion furnace. The reported MCC parameters were the averages of three measurements.

Fourier transform infrared spectroscopy (FT-IR). The FT-IR (Bruker Inc. Vector 22, coupled with an ATR accessory) was used to characterize the curing process of neat epoxy and its

PNCs in the range of 500 to 4000 cm^{-1} at a resolution of 4 cm^{-1}.

Mechanical property tests of cured epoxy nanocomposites. Dynamic mechanical analyses (DMA) measurements were carried out in the torsion rectangular mode using an AR 2000ex (TA Instrumental Company) with a strain of 0.05%, a constant frequency of 1 Hz and a heating rate of 2 °C min^{-1} in the temperature range of 30–200 °C. The sample dimensions were 12 × 3 × 40 mm^3.

Tensile tests were carried out following ASTM (Standard D 412-98a, 2002) in a unidirectional tensile testing machine (ADMET tensile strength testing system). The parameters (displacement and load) were controlled by a digital controller (MTEST Quattro) with MTESTQuattro Materials Testing Software. The samples were prepared as described for the nanocomposite fabrication in silicon rubber molds, which were designed according to the standard ASTM requirement. A crosshead speed of 1.00 mm min^{-1} was used and the strain (mm mm^{-1}) was calculated by dividing the crosshead displacement by the original gauge length.

Morphological characterizations of the Fe@C/epoxy nanocomposites and Fe@C nanostrctures. After the tensile test, the broken samples of the Fe@C/epoxy nanocomposites were collected. The morphology of the fracture surfaces and the morphology of the Fe@C nanostructures were characterized with a field emission scanning electron microscope (SEM, JEOL JSM-6700F). Before testing, the samples were first coated with a thin gold layer. And the structures of the Fe@C were further characterized by a FEI Tecnai G^2 F20 transmission electron microscopy (TEM) with a field emission gun, operated at an accelerating voltage of 200 kV. The TEM samples were prepared by drying a drop of ethanol suspension on carbon-coated copper TEM grids.

Resistivity measurements of cured Fe@C/epoxy nanocomposites

The volume resistivity was determined by measuring the DC resistance along the disc samples with diameters approximately 60 mm. An Agilent 4339B high resistance meter was used to measure the samples. This equipment allows resistivity measurements up to 10^{16} Ω. The reported values represented the mean value of eight measurements with a deviation less than 10%.

Magnetic property measurements of cured Fe@C/epoxy nanocomposites. The magnetic property measurements of the Fe@C nanoparticles and Fe@C/epoxy PNCs were carried out in a 9 T physical properties measurement system (PPMS) by Quantum Design at room temperature.

3. Results and discussion

3.1 Core–shell structured Fe@C nanoparticles

The Fe@C nanoparticles are observed to be individually separated with the particle size in the range of 10–50 nm and the carbon shell thickness about 0.5–1 nm, Fig. 1(a). The crystalline structure of the iron core of Fe@C nanoparticles is confirmed by both high resolution TEM (HRTEM) image, Fig. 1(b), and the selected area electron diffraction (SAED) pattern, Fig. 1(c). In the HTTEM image, the measured 0.21 nm lattice fringe corresponds to the (100) crystalline phase of iron (PDF#06-0696), and a thin carbon shell has covered the iron nanoparticle surface completely, which prevents the iron core from being oxidized. And in the SAED pattern, the (100) and (110) crystalline planes of iron core are clearly identified. To further confirm the composition of the nanoparticles, energy dispersive X-ray analysis (EDX) is taken in Fig. 1(d). As shown in the spectrum, only carbon, iron and copper elements can be observed. The copper element is from the TEM grid substrate and the iron and carbon elements are from the nanoparticles, the absence of oxygen element further demonstrates that the iron is well protected by the carbon shell without being oxidized.

3.2 Rheological behaviors of Fe@C/epoxy resin nanosuspensions

Fig. 2(A & B) shows the shear stress (τ) and viscosity (η) as a function of shear rate ($\partial u/\partial y$) for the pure epoxy resin and its nanosuspensions. For all these samples, η is observed inversely proportional to $\partial u/\partial y$. The fluid behaviors of the pure epoxy and its Fe@C nanosuspensions are studied by using the power law model to correlate the $\tau - \partial u/\partial y$, eqn (1):[30]

$$\tau = K(\partial u/\partial y)^n \quad (1)$$

where n is the fluid behavior index and K is consistency. For Newtonian fluids, $n = 1$, and for pseudoplastic fluid $n < 1$.[31] The values of n are summarized in Table 1. For pure epoxy resin, which is a Newtonian fluid, the n value is almost equal to 1 and the slight decrease of viscosity is attributed to the sample splashing under high rotating speed of cone.[32] However, for the nanosuspensions with Fe@C nanoparticles, the n value is observed to decrease with increasing the nanoparticle loading, indicating that the nanoparticles favor the pseudoplastic nature of the nanosuspensions, and the observed shear-thinning (shear viscosity decreases sharply with increasing the shear rate)[32] behavior is caused by the break-down of the percolated structure formed by the Fe@C nanoparticles in the nanosuspensions.[33] In addition, it is interesting to observe that compared to that of pure epoxy, the η of the nanosuspensions with 1.0 wt% Fe@C nanoparticles is decreased by almost 20% in the whole test range (0–500 1/s). A similar decreased η is also observed in the polystyrene nanosuspensions[34] and is attributed to the dilution effect of nanoparticles, which provides constraint release.[35] Due to the much shorter time scale of nanoparticles than that of the polymer molecules, instead of participating in the entanglement dynamics, nanoparticles produce a dilution effect which shown as reduced viscosity.[35] And several studies have related the decreased viscosity to the increased melt free volume resulting from the addition of the nanoparticles in the entangled and confined systems (the systems is defined by $h < R_g$, h is the average interparticle half-gap; R_g is the polymer radius of gyration),[35,36] while higher viscosity is due to the nanoparticle agglomeration.[37] For the dilution theory, studies

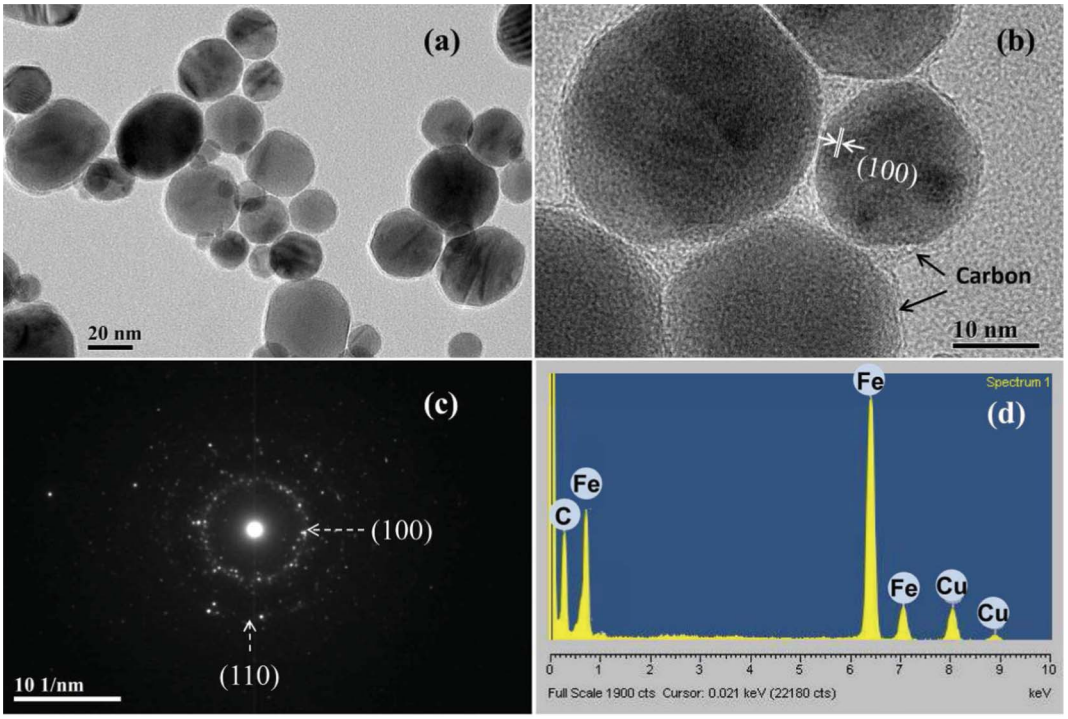

Fig. 1 (a) TEM, (b) high resolution TEM, (c) selected area electron diffraction and (d) EDAX of the Fe@C nanoparticles.

reported that the nanoparticles diffuse 100 times faster than that predicted by the Stokes–Einstein relation.[38] Compared with polymer molecules, nanoparticles show shorter time scale, which can prevent them from participating in the entanglement dynamics of bulk material and allowing them to produce a dilution effect that leads to a decreased viscosity.[35] Nanoparticles with circular shape[35] and a good dispersion were reported to decrease the nanocomposite viscosity.[37] For the Fe@C/epoxy nanosuspensions, the reduced viscosity for the 1.0 wt% Fe@C/epoxy nanosuspension indicates that at a lower loading, the nanoparticles show a dilution function in the nanosuspensions by reducing the tendency of nanosuspensions towards uncontrolled flocculation. However, with further increasing the loading of Fe@C nanoparticles, the restriction effect of the Fe@C nanoparticles on the epoxy molecular chains becomes dominated and the viscosity of the nanosuspensions is higher than that of pure epoxy resin.[39] The unusual η reduction in the spherical Fe@C nanosuspensions is beneficial for the nanocomposites processing and manufacturing, which is different from other nanofillers, like nanoclays,[40] carbon nanofibers (CNFs), and carbon nanotubes (CNTs),[41] with a significantly increased viscosity, a challenge for choosing the processing conditions.

The complex viscosity ($\eta^* = \eta' - i\eta''$, where $\eta' = G'/\omega$ and $\eta'' = G''/\omega$)[10] of the epoxy resin nanosuspensions is also studied. The absolute value of η^* ($|\eta^*| = \sqrt{(G'/\omega)^2 + (G''/\omega)^2}$) is shown in Fig. 3(A). With increasing the Fe@C nanoparticle loading, the absolute value of η^* increases, especially at low frequencies, and the increased absolute value of η^* is due to the increase of the loss modulus and the storage modulus.[42]

Fig. 3(B & C) shows the storage modulus (G') and the loss modulus (G'') as a function of frequency. Both the G' and the G'' are observed to increase with increasing frequency and nanoparticle loading, which is attributed to the interactions of the nanoparticle–nanoparticle and the nanoparticle–epoxy monomers.[37] As aforementioned, the percolation structure would be formed by the Fe@C nanoparticles in the nanosuspensions,[33] thus with increasing the nanoparticle loading, both G' and G'' curves tend to be a plateau.[43] In addition, the G' for 20.0 wt% Fe@C nanosuspensions is observed to be almost independent of the frequency, indicating the creation of a network structure formed by the intimate contact of the nanoparticles.[37,44]

3.3 Differential scanning calorimetry of cured epoxy resin and its nanocomposites

For thermosetting systems, gelation, curing, vitrification, and devitrification events can be studied with DSC tests.[45] In general, the former two processes can be observed in the uncured samples, however, if the material is not fully cured, an exothermal peak, which represents the curing process, can also be observed in the cured samples. No obvious curing peak can be observed in Fig. 4, indicating that all the samples have been well cured. The glass transition temperature (T_g) is summarized in Table 2, and for the PNCs, compared with cured pure epoxy, the existence of nanofillers in the cured epoxy resin is observed to cause a decreased T_g. In addition, T_g is observed to increase with increasing the Fe@C nanoparticle loading from 1.0 to 10.0 wt%, however, further increasing the nanoparticle loading to 20.0 wt% leads to a reduced T_g. The lower T_g in the PNCs with higher Fe@C nanoparticle loading is

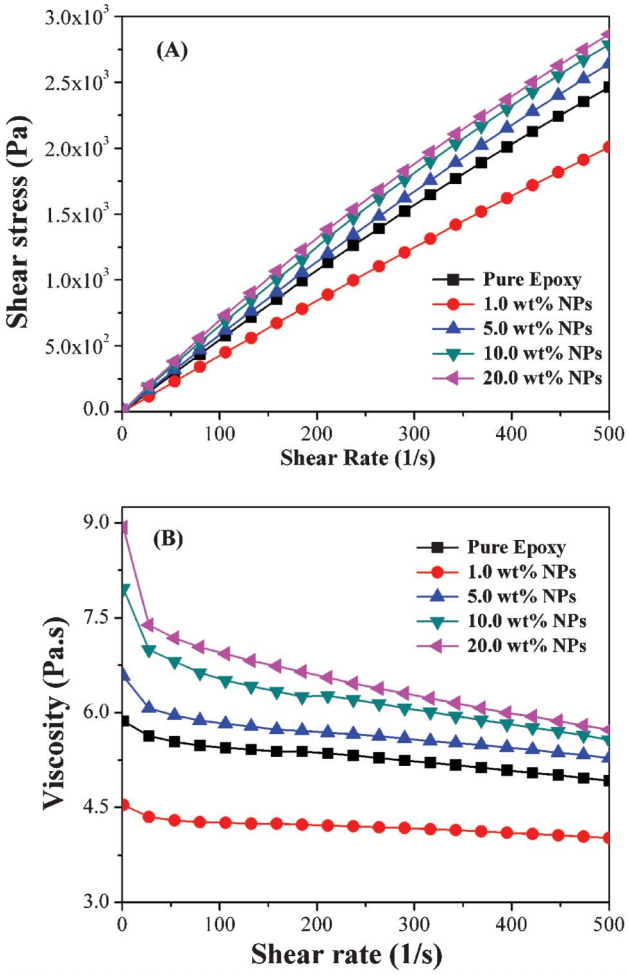

Fig. 2 (A) Shear stress and (B) viscosity *vs.* shear rate of pure epoxy and liquid Fe@C/epoxy suspension with different NPs loadings.

attributed to the enlarged free volume arising from the interface between the fillers and epoxy resin,[46] which provides more space for polymer chain segments to move even at a lower temperature. However, the structure formed by nanoparticles would restrain the movement of the epoxy polymer chains, which would lead to the enhancement of T_g. Thus, T_g is determined by the competing two factors, and at lower loading (1.0, 5.0 and 10.0 wt%), the restrained function of nanoparticles is the dominant parameter, and T_g is observed to increase with increasing nanoparticle loading. However, after percolation structure is formed, further increasing the loading of nanoparticles would only enhance the free volume effect and cause a lower T_g.

Table 1 The rheological data of pure epoxy and the liquid Fe@C/epoxy suspensions

	n
Pure epoxy	0.955 ± 0.004
1.0 wt% Fe@C/epoxy	0.923 ± 0.006
5.0 wt% Fe@C/epoxy	0.930 ± 0.005
10.0 wt% Fe@C/epoxy	0.890 ± 0.007
20.0 wt% Fe@C/epoxy	0.868 ± 0.007

3.4 Degree of curing studied by FT-IR analysis

The curing process of pure epoxy resin and its PNCs can also be studied by FT-IR spectra, Fig. 5. It is known that the variation of the epoxy groups can be reflected by the peak at 913 cm^{-1} based on the fact that the intensity of this band decreases with increasing curing extent. And the absorption peak at 1616 cm^{-1} of a benzene ring is considered as the internal standard. According to the Beer–Lambert law, the extent of curing (α) can be calculated by eqn (2):[47]

$$\alpha = \frac{A^{1610}_{\text{cured}} A^{913}_{\text{uncured}} - A^{913}_{\text{cured}} A^{1610}_{\text{uncured}}}{A^{1610}_{\text{cured}} A^{913}_{\text{uncured}}} \quad (2)$$

where A_{uncured} is the original absorbance of pure epoxy resin without curing; A_{cured} is the absorbance of cured epoxy and its PNCs. The curing extent values of pure epoxy and 10.0 wt% Fe@C/epoxy PNCs are summarized in Table 3, and 0 h represents liquid phase samples containing curing agent, which were heated at 70 °C for 2 h and were further heated at 120 °C for 5 h. It can be observed that in the liquid phase, the polymerization process had already taken place, and the curing extent value for pure epoxy and 10.0 wt% Fe@C/epoxy are almost the same. Although it is known that the nanoparticles obstruct the formation of high cross-linked molecular structure of epoxy[48,49] the almost same value of curing extent at 0 h indicating that the existence of nanoparticles shows limited impedimental effect in liquid phase. However, when heated at higher temperature (120 °C for 5 h), the polymerization is accelerated and thus the curing extent of pure epoxy becomes higher than that of 10.0 wt% Fe@C/epoxy. With the curing process proceeding, the mobility of the monomer and curing agent would decrease,[50] and the obstructive function of nanoparticles becomes a dominant factor, which caused the lower curing extent in 10.0 wt% Fe@C/epoxy PNCs than that in pure epoxy.

3.5 Thermogravimetric analysis of cured epoxy resin and its nanocomposites

Fig. 6 shows the TGA curves of the cured pure epoxy and its PNCs with Fe@C nanoparticles in air (the TGA and differential thermogravimetry (DTG) result of pure Fe@C nanoparticles is shown in Fig. S1, ESI,† and the DTG curves of pure epoxy and its PNCs are shown in Fig. S2 in ESI†). Both pure epoxy and PNCs are observed to have similar decomposition profiles and the degradation takes place in two stages. The first (T_1) and second (T_2) onset decomposition temperature, as well as the 20% weight loss temperature ($T_{20\%}$) are summarized in Table 2. Compared with that of pure epoxy, the thermal stability of the PNCs is observed to slightly decrease with a lower value of $T_{1\ \text{onset}}$, $T_{2\ \text{onset}}$, and $T_{20\%}$. In addition, the $T_{2\ \text{onset}}$ is observed to be inversely proportional to the Fe@C nanoparticle loading. The reduced thermal stability results from the spatial obstruction of the nanoparticles on the formed high cross-linked molecular structure of epoxy.[48,49] And the PNCs with limited formed network structure would be

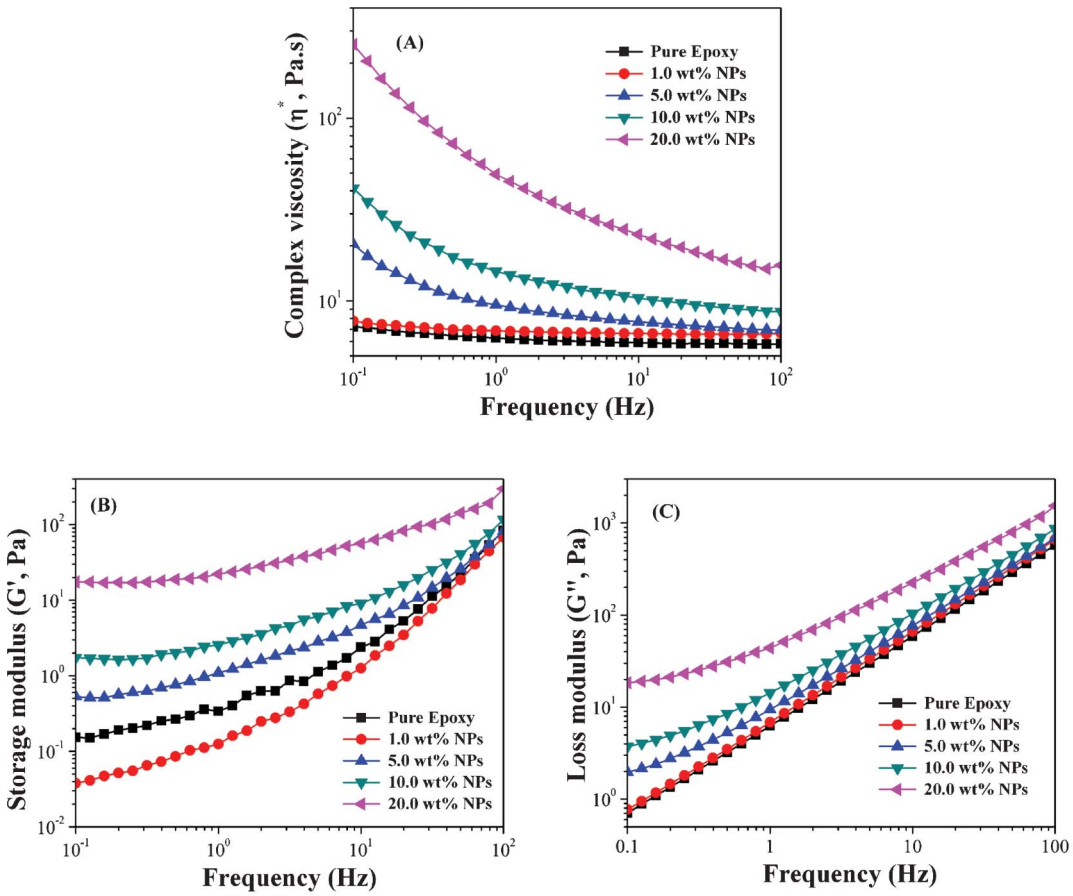

Fig. 3 (A) Complex viscosity, (B) storage modulus (*G'*) and (C) loss modulus (*G''*) *vs.* frequency of pure epoxy and Fe@C/epoxy nanosuspensions.

easily broken down with increasing temperature and thus have a decreased decomposition temperature.[51] Although the thermal stability of the PNCs decreases to some extent after the incorporation of the nanoparticles, the slight deleteriousness of the thermal stability with higher particle loading gives some essential guidance to the designing of PNCs that is required for high particle loadings to incorporate multifunctional properties, such as magnetic, electric and microwave absorption properties.[52,53]

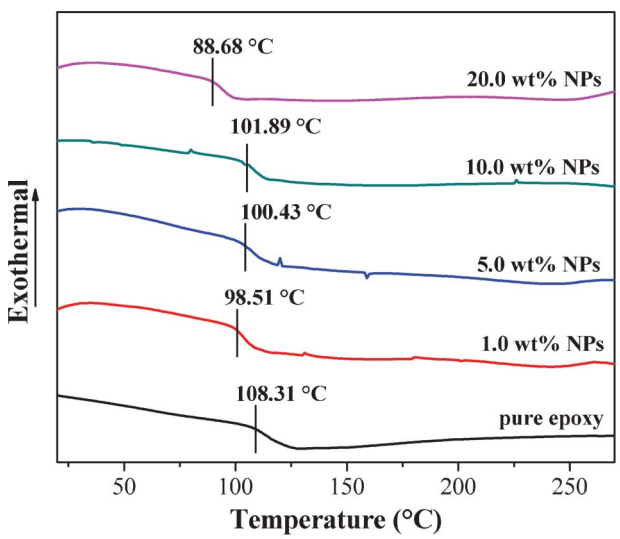

Fig. 4 DSC curves of the cured pure epoxy and its PNCs with different loading levels of Fe@C nanoparticles.

3.6 Flammability analysis of cured epoxy nanocomposites

The flammability behaviors of the cured PNCs with Fe@C nanoparticles were evaluated by studying the heat release rate (HRR) as a function of temperature, Fig. 7, and the heat release capacity (HR capacity), peak heat release rate (pHRR), total heat release (total HR) are summarized in Table 4. It is shown

Table 2 TGA results of neat cured epoxy and nanocomposites[a]

Samples	$T_{1\ onset}$ (°C)	$T_{2\ onset}$ (°C)	$T_{20\%}$ (°C)	T_g (°C)
Pure epoxy	364.5	549.8	378.6	108.31
1.0 wt% Fe@C/epoxy	355.5	491.7	368.3	98.51
5.0 wt% Fe@C/epoxy	355.4	477.3	365.8	101.89
10.0 wt% Fe@C/epoxy	354.9	470.6	364.4	100.43
20.0 wt% Fe@C/epoxy	357.7	462.9	368.4	88.68

[a] $T_{1\ onset}$ and $T_{2\ onset}$ indicate the onset degradation temperature of first and second stage, respectively. $T_{20\%}$ represents the temperature of degradation, at which the weight loss is 20%.

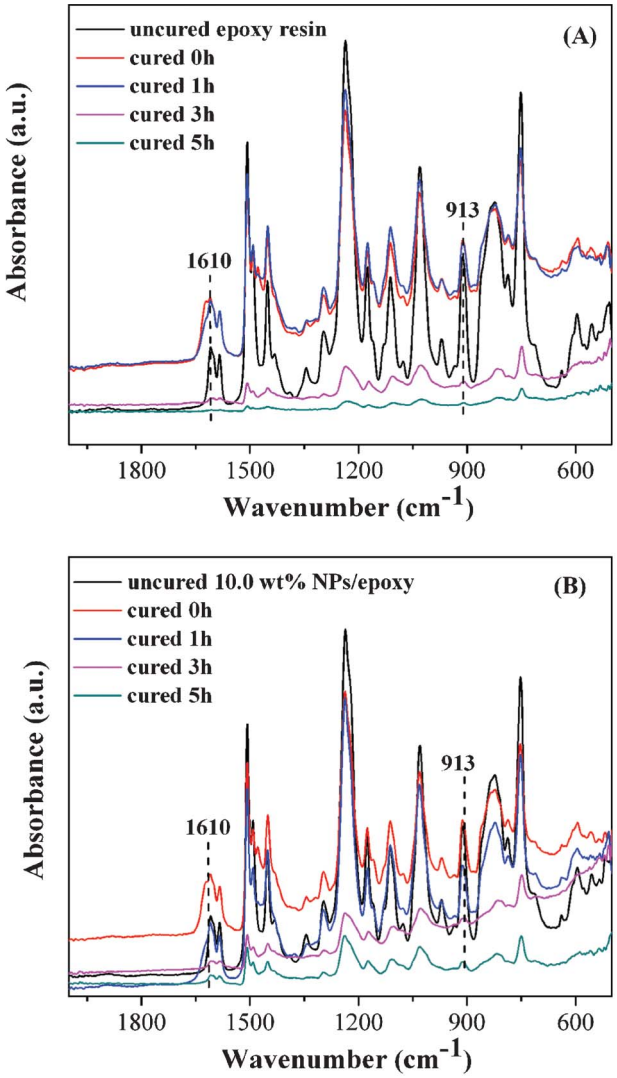

Fig. 5 FT-IR curves of the pure epoxy and its PNCs.

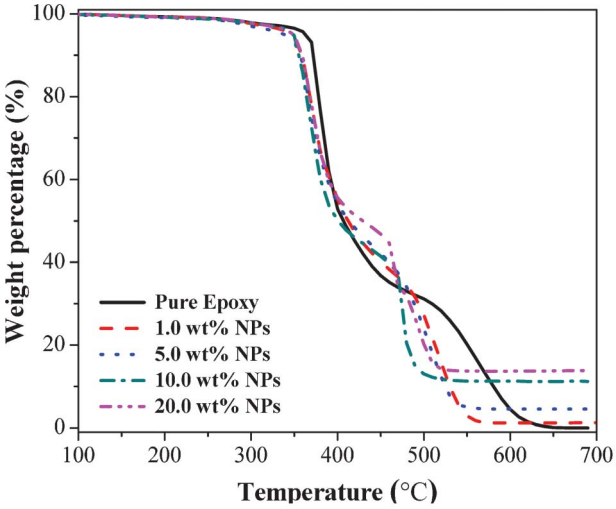

Fig. 6 Thermogravimetric analysis (TGA) curves of the pure epoxy and the PNCs.

that the values of HR capacity, pHRR and total HR all decrease with increasing the nanoparticle loading. Compared with that of pure epoxy, the pHRR value of the PNCs with 20.0 wt% Fe@C nanoparticles even is decreased by 35.18%. The lower value of these parameters indicates a reduced flammability of the PNCs, which can be attributed to the existence of Fe@C nanoparticles. Generally, metal components can favor the char formation in the organic materials by inducing an aromatization effect and reducing the reactive radicals during depolymerization process.[54,55] In addition, char residue is considered as a denotation of reduced flammability, the formed char on the surface of materials can prevent heat being transferred from the heat source to the inner material[56] and also obstruct the distribution of combustible gases produced during the burning process.[57]

Table 3 Curing extent of the pure epoxy and 10.0 wt% Fe@C/epoxy PNCs

	0 h	1 h	2 h	3 h	4 h	5 h
Pure epoxy	0.49	0.54	0.58	0.75	0.88	0.96
10.0 wt% Fe@C/epoxy	0.47	0.49	0.51	0.66	0.71	0.83

3.7 Dynamic mechanical properties of cured epoxy resin and its nanocomposites

Dynamic mechanical analysis (DMA) shows the information of the storage modulus (G'), loss modulus (G'') and tanδ in the testing temperature range. The storage modulus represents the elastic behavior or the energy storage in the nanocomposites, while the loss modulus reflects the viscous behavior or the energy dissipation in the nanocomposites during the test.[58,59] Fig. 8(A & B) shows the G' and G'' for the cured pure epoxy resin and its PNCs. In the glass plateau (below 100 °C, when the polymer chains are unable to make any movement), the values of G'' are almost the same for all the samples. However, the PNCs with 20 wt% Fe@C nanoparticles show a

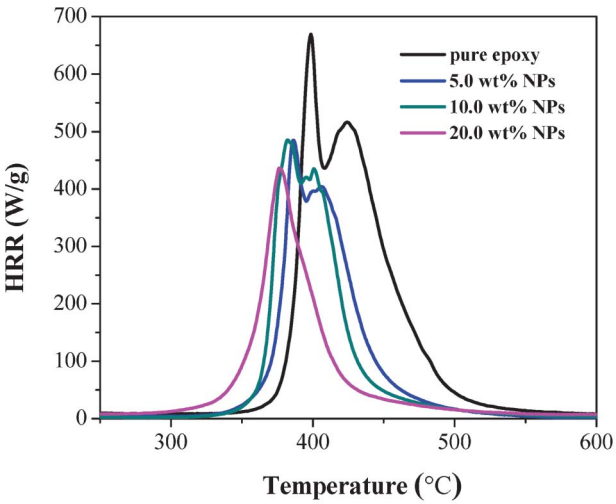

Fig. 7 The HRR *vs.* temperature curves of the cured pure epoxy and its PNCs.

Table 4 Heat release capacity (HR capacity), peak heat release rate (pHRR), total heat release and char residue for the cured pure epoxy and its PNCs

	HR capacity (J g^{-1} K^{-1})	Peak HRR (W g^{-1})	Total HR (kJ g^{-1})
Pure epoxy	491	664.3	28.0
5.0 wt% Fe@C/epoxy	444	479.9	23.2
10.0 wt% Fe@C/epoxy	441	483.6	23.3
20.0 wt% Fe@C/epoxy	393	430.6	19.0

much higher G' than pure epoxy, the enhanced G' is due to the confinement and relatively uniform dispersion of the Fe@C nanoparticles in the matrix.[58] In addition, in the glass transition process (100–150 °C), compared with pure epoxy, the sharp decrease of G' is delayed by 10–20 °C in the PNCs, the improved thermo-mechanical properties are attributed to the network structure formed by the Fe@C nanoparticles in the polymer matrix, which restricts the mobility of the main chains of the epoxy resin.[58] With the temperature further increased to rubber plateau (above 150 °C), the G'' for the PNCs is observed to increase with increasing the Fe@C nanoparticle loading. In the rubber plateau, the polymer chains are free to make movement, the existence of the Fe@C nanoparticles would cause an enlarged friction between Fe@C NPs and polymer chains,[60] and the heat created during the friction would lead to higher energy dissipation.

The tanδ is the ratio of the G'' to the G', and the peak of tanδ is often used to determine the glass transition temperature, T_g. As shown in Fig. 8(C), the peak position of the PNCs is observed to shift towards a higher temperature as compared to that of pure epoxy. This shift indicates an interaction between epoxy and the Fe@C nanoparticles.[61] Changes in the thermal and mechanical properties of the reinforced PNCs are important indicators of the percolation of the nanofillers.[32] A lower T_g is also observed, Fig. 8(C), when the nanoparticle loading is increased to 20 wt%. Increasing the nanoparticle loading leads to a slight nanoparticle agglomeration, Fig. 10(f), which introduces more free volume and chain mobility near

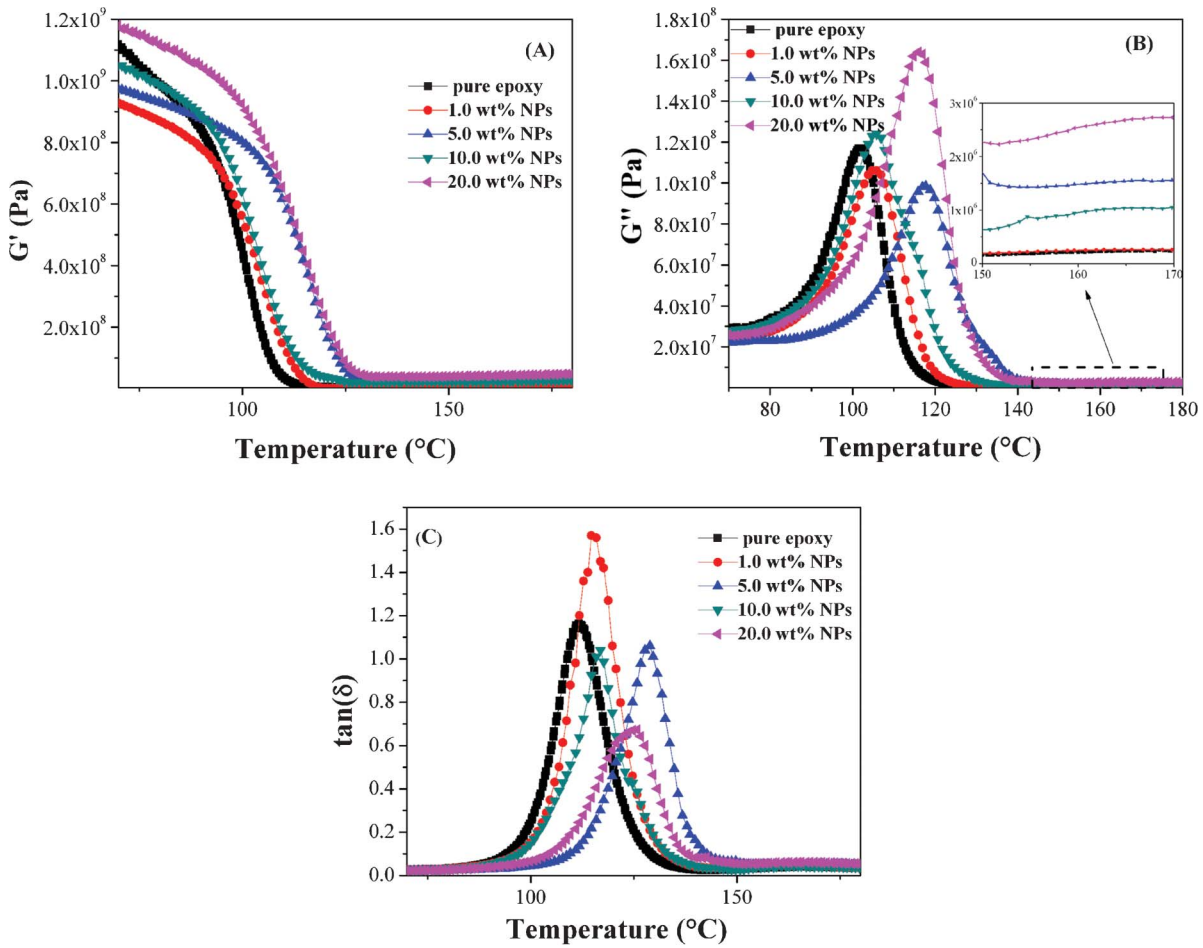

Fig. 8 (A) Storage modulus (G'), (B) loss modulus (G'') and (C) tanδ *vs.* temperature curves for nanocomposites with different Fe@C loadings.

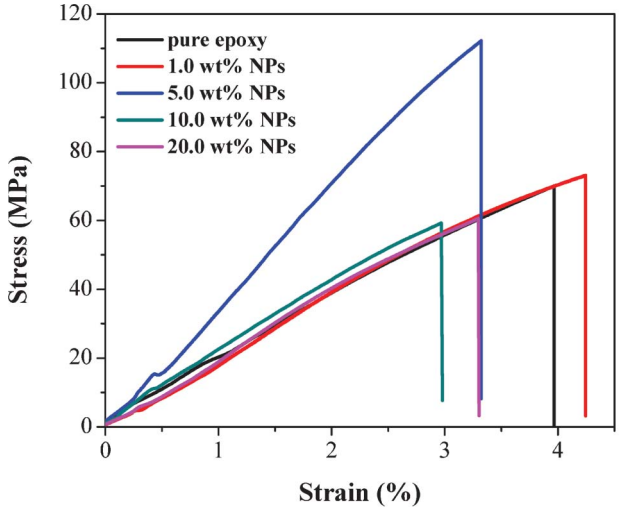

Fig. 9 Stress–strain curves of cured epoxy nanocomposites filled with different loadings of Fe@C nanoparticles.

the particles.[61,62] This leads to a lower T_g for the PNCs with higher Fe@C loadings.

3.8 Tensile mechanical property and fracture surface analysis of cured nanocomposites

The curves of tensile stress as a function of strain are shown in Fig. 9. The tensile strength of the PNCs first increases and then decreases with increasing the Fe@C nanoparticle loading, and the highest strength is shown in the 5.0 wt% Fe@C/epoxy PNCs, with a value of 112.2 MPa, which is 60% higher than that of pure epoxy (69.4 MPa). The enhanced tensile strength is attributed to the microcrazing initiated by the nanoparticles, which can relieve the stress state and limit the void formation in the bulk polymer.[63,64] Different morphologies are observed in the SEM image of the fracture surface, Fig. 10. The surface for pure epoxy is very smooth reflecting a typical brittle fracture; however, the PNCs show a rough fracture surface. A rough surface can be attributed to the matrix shear yielding or the polymer deformation between the Fe@C nanoparticles, which were also observed in the alumina NPs reinforced vinyl ester resin nanocomposites[65] and carbon nanofibers filled epoxy nanocomposites.[58] As can be seen in Fig. 10(b), the fracture surface exhibits a large number of micro-cracks, which are detrimental to the internal stress transfer while an external force load is applied. However, with increasing the nanoparticle loading to 5.0 wt%, Fig. 10(e), the fracture surface exhibits a good dispersion of the nanoparticles accompanied by a small number of microcrazing, indicating that the stress is randomly distributed with the aid of Fe@C nanoparticles.[58] In addition, no particle agglomeration could be observed in the 5.0 wt% Fe@C/epoxy PNCs. However, with further increasing the nanoparticle loading to 20.0 wt%, severe agglomeration could be observed in Fig. 10(f), defects can be formed in the nanoparticle rich region and initiate the failure,[66] which in turn decreases the tensile strength. At the same time, the ''island'' structures formed by nanoparticles embedded in the epoxy matrix (marked with solid circles) are

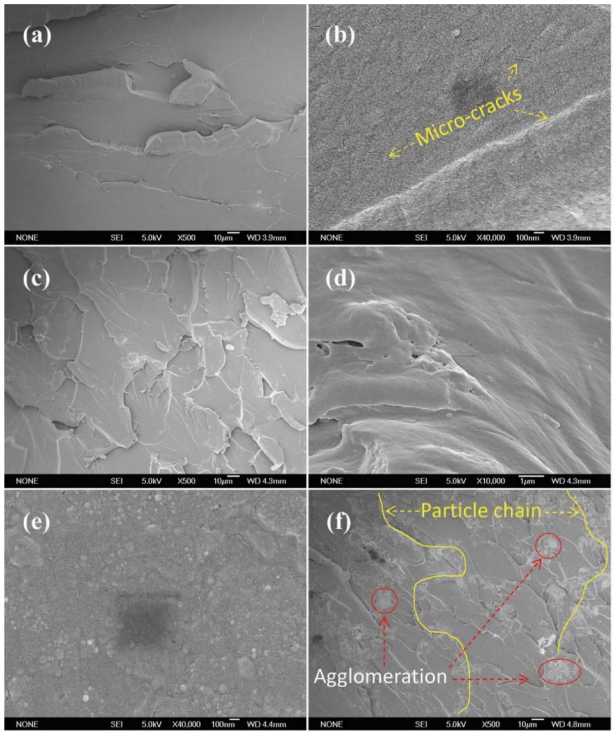

Fig. 10 SEM microstructure of the fracture surface of (a & b) pure epoxy, (c & d) 1.0 wt% Fe@C/epoxy, (e) 5.0 wt% Fe@C/epoxy and (f) 20.0 wt% Fe@C/epoxy PNCs.

connected from each other to form a chain-like morphology as marked with solid line in Fig. 10(f). These chain structures play an important role in electron transportation within the PNCs and would significantly reduce the conductivity, which will be discussed later.

3.9 Electrical conductivity (σ) of cured epoxy nanocomposites

The electrical conductivity of cured epoxy and the PNCs is studied through the measurement of the volume resistivity. As shown in Fig. 11, the resistivity is observed to decrease with increasing the Fe@C nanoparticle loading, however, the extent of reduction is not linearly inversely proportional to the nanoparticle loading. Firstly, the resistivity was observed to significantly decrease from 7.8×10^{13} ohm cm for pure epoxy to 15.7×10^{7} ohm cm for the PNCs with 10.0 wt% nanoparticle loading, while, with further increasing the nanoparticle loading to 20.0 wt%, the resistivity is decreased gently to 1.2×10^{6} ohm cm. The variation of resistivity indicates the formation of percolation network. At lower loadings, the nanoparticles are highly dispersed and rarely touch each other, the electron hopping between nanoparticles is relatively difficult due to the large spacing,[67] thus, resistivity would decrease sharply with increasing the nanoparticle loading. And at certain loading, the nanoparticles can construct a network in the polymer matrix, which is often called percolation threshold allowing the electron transportation between neighboring nanoparticles[68] and thus a huge decrease in the resistivity is observed.

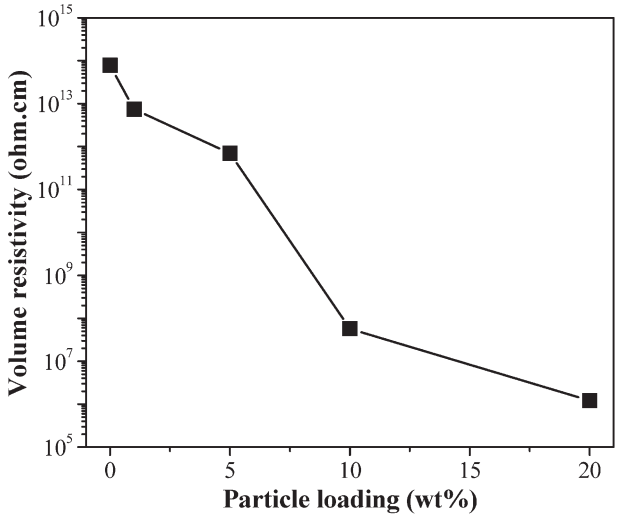

Fig. 11 Volume resistivity of the cured pure epoxy and its PNCs with different loading levels of Fe@C nanoparticles.

3.10 Magnetic property of cured epoxy nanocomposites

Fig. 12 shows the room temperature hysteresis loops of the pure Fe@C nanoparticles and the cured epoxy PNCs with 5.0 wt% Fe@C nanoparticles. The saturation magnetization (M_s) reaches at 35 and 5 emu g^{-1} for pure Fe@C NPs and 5.0 wt% Fe@C/epoxy PNCs, respectively. And with the nanoparticles dispersed in the polymer matrix, the field required to saturate becomes much lower. In addition, the coercivity (H_c, Oe) represents the external applied magnetic field that is required to return the material to zero magnetization condition and the remnant magnetization (M_r) represents the residue magnetization after the applied field is reduced to zero. Both H_c and M_r are read from the axes crossover points and clearly shown in Fig. 12 (inset figures). As compared to pure Fe@C nanoparticles (200 Oe), the significantly increased H_c of the PNCs with 5.0 wt% Fe@C NPs (353.5 Oe) indicates that the Fe@C nanoparticles become magnetically harder after dispersing in epoxy. And this kind of variation of the Fe@C nanoparticles is due to the enlarged spacer distance for the single domain particles in the polymer matrix,[69,70] which causes the reduction of interparticle dipolar interaction, as compared to the closer contact for the pure Fe@C nanoparticles.

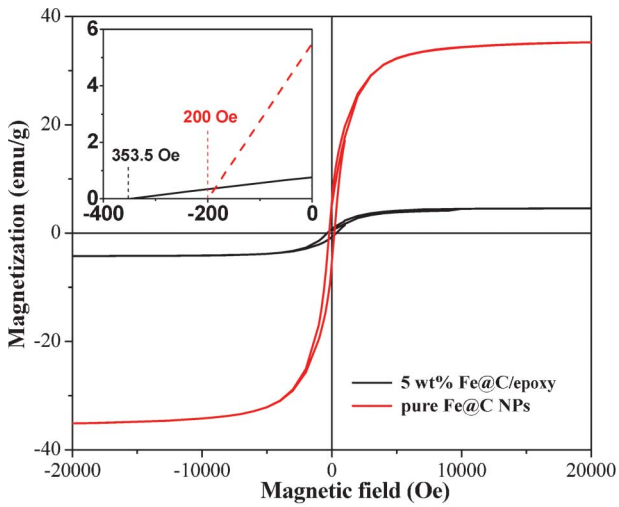

Fig. 12 Hysteresis loops of the Fe@C NPs and the 5.0 wt% Fe@C/epoxy PNCs.

4. Conclusions

The magnetic nanocomposites filled with different loading levels of the Fe@C nanoparticles have been prepared and systematically studied. The rheological behavior of the Fe@C/epoxy nanosuspensions shows a tendency toward non-Newtonian behavior with increasing Fe@C nanoparticle loading, and the special phenomenon is attributed to the percolation structure formed by the Fe@C nanoparticles, in addition, the decreased viscosity in the epoxy nanosuspensions at 1.0 wt% Fe@C nanoparticle loading is attributed to the dilution effect of the nanoparticles in the polymer nanosuspensions. The curing process is studied by FT-IR analysis and the result indicates that the PNCs have lower curing extent than pure epoxy and the nanoparticles would obstruct the curing process. The dynamic mechanical analysis (DMA) of the cured Fe@C/epoxy PNCs shows an enhanced storage modulus at higher nanoparticle loading due to the confinement effect of the Fe@C nanoparticles on the polymer matrix. TGA results demonstrated a decreased thermal stability of the Fe@C/epoxy PNCs as compared to that of the pure epoxy, which is attributed to the spatial obstruction of nanoparticles on the formation of high cross-linked molecular structure of epoxy. However, due to the easy char formation from the organic materials induced by metal components, the PNCs show lower HRR and pHRR and reduced flammability. Up to 60% increment of tensile strength is observed in the PNCs with 5.0 wt% Fe@C nanoparticles due to the microcrazing initiated by the nanoparticles, and the particle chains formed in the polymer matrix are also observed in the fracture surface of the PNCs. Finally, the conductive and magnetic epoxy PNCs are achieved through the dispersion of Fe@C nanoparticles in the cured epoxy nanocomposites. Huge decrease in the resistivity of the PNCs is observed indicating the formation of a conductive network upon the addition of Fe@C nanoparticles. The saturation magnetization of the Fe@C/epoxy PNCs reaches at a lower magnetic field compared to that of pure Fe@C nanoparticles, while the coercivity of the PNCs increases significantly, indicating that the Fe@C nanoparticles become magnetically harder after dispersing in the polymer matrix.

Acknowledgements

This work is supported by the National Science Foundation–Nanoscale Interdisciplinary Research Team and Materials Processing and Manufacturing (CMMI 10-30755). D. P.

Young acknowledges support from the NSF under Grant No. DMR 10-05764.

References

1 J. Zhu, S. Wei, J. Ryu, L. Sun, Z. Luo and Z. Guo, *ACS Appl. Mater. Interfaces*, 2010, **2**, 2100–2107.
2 H. Gu, S. Tadakamalla, Y. Huang, H. A. Colorado, Z. Luo, N. Haldolaarachchige, D. P. Young, S. Wei and Z. Guo, *ACS Appl. Mater. Interfaces*, 2012, **4**, 5613–5624.
3 M. A. Soto-Oviedo, O. A. Araújo, R. Faez, M. C. Rezende and M.-A. de Paoli, *Synth. Met.*, 2006, **156**, 1249–1255.
4 Z. Guo, S. Park, H. T. Hahn, S. Wei, M. Moldovan, A. B. Karki and D. P. Young, *J. Appl. Phys.*, 2007, **10**, 09M511.
5 X. Wang, L. Wang, X. He, Y. Zhang and L. Chen, *Talanta*, 2009, **78**, 327–332.
6 M. Fini, G. Giavaresi, N. N. Aldini, P. Torricelli, R. Botter, D. Beruto and R. Giardino, *Biomaterials*, 2002, **23**, 4523–4531.
7 V. B. Mišković-Stanković, M. R. Stanić and D. M. Dražić, *Prog. Org. Coat.*, 1999, **36**, 53–63.
8 C.-S. Wang and J.-Y. Shieh, *J. Appl. Polym. Sci.*, 1999, **73**, 353–361.
9 Y. Li and C. P. Wong, *Mater. Sci. Eng., R*, 2006, **51**, 1–35.
10 H. Gu, S. Tadakamalla, X. Zhang, Y.-D. Huang, Y. Jiang, H. A. Colorado, Z. Luo, S. Wei and Z. Guo, *J. Mater. Chem. C*, 2013, **1**, 729–743.
11 A. A. Novakovaa, V. Y Lanchinskayaa, A. V. Volkova, T. S. Gendlerb, M. A. M. T. Y. Kiselevaa and S. B. Zezina, *J. Magn. Magn. Mater.*, 2003, **258–259**, 354–357.
12 L. Zhao, B. Pan, W. Zhang, S. Zhang and Q. Zhang, *Chem. Eng. J.*, 2011, **170**, 381–394.
13 S. Wei, Q. Wang, J. Zhu, L. Sun, H. Lin and Z. Guo, *Nanoscale*, 2011, **3**, 4474–4502.
14 B. Wetzel, F. Haupert and M. Q. Zhang, *Compos. Sci. Technol.*, 2003, **63**, 2055–2067.
15 J.-Y. Lee, Y. Liao, R. Nagahata and S. Horiuchi, *Polymer*, 2006, **47**, 7970–7979.
16 H. Wu, Z. Zhao and X. Yao, *J. Phys. D: Appl. Phys.*, 2000, **33**, 2398–2401.
17 J. Zhu, S. Wei, N. Haldolaarachchige, D. P. Young and Z. Guo, *J. Phys. Chem. C*, 2011, **115**, 15304–15310.
18 J. Zhu, S. Wei, I. Y. Lee, S. Park, J. Willis, N. Haldolaarachchige, D. P. Young, Z. Luo and Z. Guo, *RSC Adv.*, 2012, **2**, 1136–1143.
19 M. Chen, H. Qu, J. Zhu, Z. Luo, A. Khasanov, A. S. Kucknoor, N. Haldolaarachchige, D. P. Young, S. Wei and Z. Guo, *Polymer*, 2012, **53**, 4501–4511.
20 J. L. Wilson, P. Poddar, N. A. Frey, H. Srikanth, K. Mohomed, J. P. Harmon, S. Kotha and J. Wachsmuth, *J. Appl. Phys.*, 2004, **95**, 1439–1443.
21 S. R. Rudge, T. L. Kurtz, C. R. Vessely, L. G. Catterall and D. L. Williamson, *Biomaterials*, 2000, **21**, 1411–1420.
22 D. Zhang, S. Wei, C. Kaila, X. Su, J. Wu, A. B. Karki, D. P. Young and Z. Guo, *Nanoscale*, 2010, **2**, 917–919.
23 J. Zhu, M. Chen, N. Yerra, N. Haldolaarachchige, S. Pallavkar, Z. Luo, T. C. Ho, J. Hopper, D. P. Young, S. Wei and Z. Guo, *Nanoscale*, 2013, **5**, 1825–1830.
24 Z. Guo, M. Moldovan, D. P. Young, L. L. Henry and E. J. Podlaha, *Electrochem. Solid-State Lett.*, 2007, **10**, E31–E35.
25 Z. Lu, M. D. Prouty, Z. Guo, V. O. Golub, C. S. S. R. Kumar and Y. M. Lvov, *Langmuir*, 2005, **21**, 2042–2050.
26 Y. Xu, S. Palchoudhury, Y. Qin, T. Macher and Y. Bao, *Langmuir*, 2012, **28**, 8767–8772.
27 J. Hassoun, G. Derrien, S. Panero and B. Scrosati, *Adv. Mater.*, 2008, **20**, 3169–3175.
28 S. X. Wang, N. X. Sun, M. Yamaguchi and S. Yabukami, *Nature*, 2000, **407**, 150–151.
29 R. F. H Kronmüller, M. Seeger and A. Zern, *J. Phys. D: Appl. Phys.*, 1996, **29**, 2274–2283.
30 R. M. Manglik and P. Fang, *Int. J. Heat Mass Transfer*, 2002, **45**, 803–814.
31 X. Zhang, Q. He, H. Gu, S. Wei and Z. Guo, *J. Mater. Chem. C*, 2013, **1**, 2886.
32 X. Zhang, Q. He, H. Gu, H. A. Colorado, S. Wei and Z. Guo, *ACS Appl. Mater. Interfaces*, 2013, **5**, 898–910.
33 M. Abdalla, D. Dean, D. Adibempe, E. Nyairo, P. Robinson and G. Thompson, *Polymer*, 2007, **48**, 5662–5670.
34 M. E. Mackay, T. T. Dao, A. Tuteja, D. L. Ho, B. Van Horn, H.-C. Kim and C. J. Hawker, *Nat. Mater.*, 2003, **2**, 762–766.
35 A. Tuteja, P. M. Duxbury and M. E. Mackay, *Macromolecules*, 2007, **40**, 9427–9434.
36 S. Jain, J. G. P. Goossens, G. W. M. Peters, M. van Duin and P. J. Lemstra, *Soft Matter*, 2008, **4**, 1848–1854.
37 J. Zhu, S. Wei, A. Yadav and Z. Guo, *Polymer*, 2010, **51**, 2643–2651.
38 K. N. K. R. Srivastava, *J. Chem. Eng. Data*, 2009, **54**, 1452–1456.
39 D. R. Paul and L. M. Robeson, *Polymer*, 2008, **49**, 3187–3204.
40 B. Lepoittevin, M. Devalckenaere, N. Pantoustier, M. Alexandre, D. Kubies, C. Calberg, R. Jérôme and P. Dubois, *Polymer*, 2002, **43**, 4017–4023.
41 C. A. Mitchell, J. L. Bahr, S. Arepalli, J. M. Tour and R. Krishnamoorti, *Macromolecules*, 2002, **35**, 8825–8830.
42 P. Pötschke, T. D. Fornes and D. R. Paul, *Polymer*, 2002, **43**, 3247–3255.
43 S. Gurvich, *Search of Excellence, 1 edn*, CRC Press, 1991, 91, 1158.
44 M. A. Paglicawan and J. K. Kim, *Polym. Eng. Sci.*, 2008, **48**, 1667–1673.
45 G. Wisanrakkit, J. K. Gillham and J. B. Enns, *J. Appl. Polym. Sci.*, 1990, **41**, 1895–1912.
46 Y. Sun, Z. Zhang, K.-S. Moon and C. P. Wong, *J. Polym. Sci., Part B: Polym. Phys.*, 2004, **42**, 3849–3858.
47 Z. Wang, X. Yang, Q. Wang, H. T. Hahn, S.-G. Lee, K.-H. Lee and Z. Guo, *Int. J. Smart Nano Mater.*, 2011, **2**, 176–193.
48 Y. Pan, Y. Xu, L. An, H. Lu, Y. Yang, W. Chen and S. Nutt, *Macromolecules*, 2008, **41**, 9245–9258.
49 Y. Shi, S. Peterson and D. Y. Sogah, *Chem. Mater.*, 2007, **19**, 1552–1564.
50 T. F. Scott, W. D. Cook and J. S. Forsythe, *Eur. Polym. J.*, 2008, **44**, 3200–3212.
51 K. Dušek, *Epoxy Resins and Composites III*, Springer, Berlin Heidelberg, 1986, 78, 1–59.
52 Z. Guo, S. E. Lee, H. Kim, S. Park, H. T. Hahn, A. B. Karki and D. P. Young, *Acta Mater.*, 2009, **57**, 267–277.
53 Z. Guo, S. Park, S. Wei, T. Pereira, M. Moldovan, A. B. Karki, D. P. Young and H. T. Hahn, *Nanotechnology*, 2007, **18**, 335701–335708.

54 Q. He, T. Yuan, X. Zhang, Z. Luo, N. Haldolaarachchige, L. Sun, D. P. Young, S. Wei and Z. Guo, *Macromolecules*, 2013, **46**, 2357–2368.
55 D.-Y. Wang, Y. Liu, Y.-Z. Wang, C. P. Artiles, T. R. Hull and D. Price, *Polym. Degrad. Stab.*, 2007, **92**, 1592–1598.
56 J. W. Gilman, *Appl. Clay Sci.*, 1999, **15**, 31–49.
57 Y. L. Liu, *Polymer*, 2001, **42**, 3445–3454.
58 J. Zhu, S. Wei, J. Ryu, M. Budhathoki, G. Liang and Z. Guo, *J. Mater. Chem.*, 2010, **20**, 4937–4948.
59 B. Fabry, G. N. Maksym, J. P. Butler, M. Glogauer, D. Navajas and J. J. Fredberg, *Phys. Rev. Lett.*, 2001, **87**, 148102.
60 X. Chen, S. Wei, A. Yadav, R. Patil, J. Zhu, R. Ximenes, L. Sun and Z. Guo, *Macromol. Mater. Eng.*, 2011, **296**, 434–443.
61 R. Q. Lesley, M. Hamming and P. B. M. Brinson, *Compos. Sci. Technol.*, 2009, **69**, 1880–1886.
62 C. S. Sherely, A. Paul, K. Joseph and G. D. G. Mathew, *et al.*, *Polym. Eng. Sci.*, 2010, **50**, 384.
63 B. J. Ash, R. W. Siegel and L. S. Schadler, *Macromolecules*, 2004, **37**, 1358–1369.
64 Y. Sha, C. Y. Hui, A. Ruina and E. J. Kramer, *Macromolecules*, 1995, **28**, 2450–2459.
65 Z. Guo, T. Pereira, O. Choi, Y. Wang and H. T. Hahn, *J. Mater. Chem.*, 2006, **16**, 2800–2808.
66 I. Isik, U. Yilmazer and G. Bayram, *Polymer*, 2003, **44**, 6371–6377.
67 J. Zhu, S. Wei, Y. Li, L. Sun, N. Haldolaarachchige, D. P. Young, C. Southworth, A. Khasanov, Z. Luo and Z. Guo, *Macromolecules*, 2011, **44**, 4382–4391.
68 L. I. Trakhtenberg, E. Axelrod, G. N. Gerasimov, E. V. Nikolaeva and E. I. Smirnova, *J. Non-Cryst. Solids*, 2002, **305**, 190–196.
69 Z. Guo, K. Lei, Y. Li, H. W. Ng, S. Prikhodko and H. T. Hahn, *Compos. Sci. Technol.*, 2008, **68**, 1513–1520.
70 D. Zhang, A. B. Karki, D. Rutman, D. P. Young, A. Wang, D. Cocke, T. H. Ho and Z. Guo, *Polymer*, 2009, **50**, 4189–4198.

